## PAPER

Check for updates

# Melatonin loaded PLGA nanoparticles effectively ameliorate the *in vitro* maturation of deteriorated oocytes and the cryoprotective abilities during vitrification process†

Sujin Lee, Hye Jin Kim, Hui Bang Cho, Hye-Ryoung Kim, Sujeong Lee, Ji-In Park and Keun-Hong Park ⓘ *

Almost all cells can be exposed to stress, but oocytes, which are female germ cells, are particularly vulnerable to damage. In this study, melatonin, a well-known antioxidant, was loaded into biodegradable poly (lactic-*co*-glycolic acid) (PLGA) nanoparticles (NPs) and delivered to damaged oocytes in order to improve their quality and restoration. Etoposide (ETP)-induced deteriorated oocytes show poor maturity, mitochondrial aggregation, and DNA damage. Treatment of NPs not only reduced DNA damage but also improved mitochondrial stability, as evidenced by increased ATP levels and mitochondrial homogeneity. When melatonin was added to the culture medium at the same concentration as that present in NPs, DNA and mitochondrial repair was insignificant due to the half-life of melatonin, whereas DNA repair in damaged oocytes upon multiple treatments with melatonin was similar to that observed with melatonin-loaded NPs. Next, we evaluated whether the oocytes treated with NPs could have cryoprotective abilities during vitrification/thawing. Vitrified-oocytes were stored at −196 °C for 0.25 h (T1) or 0.5 h (T2). After thawing, live oocytes were subjected to *in vitro* maturation. The NP-treated group showed maturity similar to the control group (77.8% in T1, 72.7% in T2) and the degree of DNA damage was reduced compared to the ETP-induced group ($p < 0.05$).

## 1. Introduction

Oocytes, which are a class of germ cells, undergo maturation in response to gonadotropin hormones (*e.g.*, follicle-stimulating hormone and luteinizing hormone) in follicles in the ovary.[1] In general, females are born with about 1 million oocytes, and follicles in the ovary develop during each reproductive cycle. Only one oocyte matures and ovulates from a follicle during each cycle. Therefore, only a few of the many oocytes present at birth mature, and most of them degenerate.[2,3] Oocytes remain in the body for up to several decades and are therefore easily damaged by the environment or external stimuli such as a pH change and reactive oxygen species (ROS) generation.[4–6] These factors reduce the quality and genetic stability of oocytes.[7,8] Exposure of cells to a variety of external and internal stimuli can induce severe DNA damage.[9] DNA double-strand breaks (DSBs) are the most pro-

blematic type of DNA damage in cells and cause mutations and chromosomal misalignment. In addition, DSBs can lead to genomic instability if erroneous repair occurs or to apoptosis if repair does not occur.[10–13] Many DSBs are induced upon exposure of oocytes to various external and internal stimuli. DNA repair in damaged oocytes is of paramount importance to maintain optimal fertility for a considerable duration and to prevent genetic defects from being passed on to the next generation.[14]

Numerous mitochondria are generated in oocytes and passed onto preimplantation embryos. To generate sufficient mitochondria to be passed onto embryos, oocytes produce an enormous number of mitochondria during the follicular stage.[15,16] Although mitochondria are the dominant organelles in the cytoplasm of oocytes, most do not participate in metabolic activities due to their shapes being small and round, and the lack of structured cristae.[17,18] These structural differences make them different from the active mitochondria found in normal somatic cells, which produce high levels of ATP.[19,20] Mitochondria present in oocytes participate in embryonic development by functioning as physiological regulators.[21–26] Mitochondrial dysfunction is considered an important contributing factor in a variety of physiopathological situations and

*Department of Biomedical Science, College of Life Science, CHA University, 6F, CHA Bio-Complex, 335 Pangyo-ro, Bundang-gu, Seongnam-si, 134-88, Republic of Kore. E-mail: pkh0410@cha.ac.kr*

apoptosis. And mitochondrial dysfunction in oocytes is a cause of infertility and has been suggested to delay and arrest the development of preimplantation embryos. Therefore, preventing mitochondrial dysfunction could be an effective therapeutic strategy for cellular degenerative processes.[27–29]

Melatonin (*N*-acetyl-5-methoxytryptamine), a major secretory product of the pineal gland, is a well-known antioxidant and therefore an effective protector of mitochondrial bioenergetic function. Melatonin is a conserved molecule derived from tryptophan found in all organisms, from unicellular organisms to vertebrates.[30,31] Melatonin act as a ROS scavenger and it reportedly prevents mitochondrial dysfunction caused by oxidative damage.[32–35] Melatonin protects mitochondria by preserving the mitochondrial membrane potential at an appropriate level and increasing ATP production by regulating the activity of complexes in the mitochondrial electron transport chain.[36,37] Also, it acts to inhibit mitochondrial permeability transition pores involved in calcium and cytochrome c release from mitochondria and plays a role in regulating the gene expression of antioxidant-related enzymes.[38–40] Melatonin has also been reported to be involved in DNA damage repair, with cells pre-treated with melatonin having significantly shorter olive tail moments when exposed to mutagenic methyl methanesulfonate (MMS) than cells that were not. This indicates that melatonin treatment increases the DNA repair capacity.[41,42] In addition, melatonin plays a crucial role in vitrified-warm oocytes for better *in vitro* maturation.[43]

As interest in fertility preservation has risen, many studies have been reported on the cryopreservation of oocytes in the assisted reproduction for fertility preservation. However, if cryopreservation is not performed under suitable conditions, cells may undergo a series of alterations such as osmotic pressure, mechanical stress, or ROS-induced injury, which leads to cell damage and even cell apoptosis. It has been reported that the addition of melatonin to a cryoprotectant or medium improves the viability and fertility of germ cells, but no studies have been conducted on the cryoprotective ability of post-thaw oocytes after the introduction of melatonin into the cells.[44–47]

Here, we treated damaged oocytes with melatonin alone or melatonin-loaded poly(lactic-*co*-glycolic acid) (PLGA) nanoparticles (NPs) to relieve the loss of oocyte quality due to mitochondrial and DNA damage, which can occur during oocyte maturation (Scheme 1). In previous studies, we conducted a study on the delivery of extracellular molecules into oocytes. Three types of nanoparticles were selected as material delivery carriers, as follows: inorganic particles (quantum dots), membrane-like liposomes (PEG/PL), and organic particles (PLGA).[48] The delivery of external substances using PLGA NPs has less cytotoxicity and more effective delivery of molecules into the oocyte. Therefore, we selected PLGA nanoparticles as melatonin drug delivery carriers based on previous studies, and in addition, in this study, the sustainable drug release effect of nanoparticles was explored by comparing the effects of melatonin alone and multiple treatments with drug delivery using nanoparticles. Conventional administration of melatonin only affects oocytes for a short duration, and its efficacy is lost over time. On the other hand, drug delivery systems in which melatonin is continuously released from the NPs mitigate DNA and mitochondrial damage much more efficiently than conventional melatonin treatment. In addition, this system avoids the need to administer melatonin several times due to its half-life. In summary, this drug delivery system can improve the quality of damaged oocytes by effectively alleviating DNA and mitochondrial damage. It also protects against cellular damage that may occur during the vitrification and thawing of oocytes.

## 2. Methods

### 2.1 Materials

Resomer® RG 503 H, poly (D,L-lactide-*co*-glycolide), melatonin (M5250), ETP (E1383), TRITC mixed isomers (87918), 3-isobutyl-1-methylxanthine (IBMX, I7018), polyvinyl alcohol (PVA, 13–23 kDa, 363170), M2 medium (M7167), M16 medium (M7292), PBS (P4417-100TAB), dimethyl sulfoxide (DMSO, D2650), and bovine serum albumin (BSA, B4287) were purchased from Sigma-Aldrich (St. Louis, MO, USA). Dulbecco's modified Eagle's medium, high glucose (DMEM-high), was purchased from HyClone (Logan, Canada). The antibiotic–antimycotic solution (15240062) was purchased from Thermo Fisher Scientific (Waltham, MA, USA).

### 2.2 Synthesis of melatonin-loaded NPs

Melatonin/TRITC-loaded PLGA NPs were fabricated using a water-in-oil-in-water solvent evaporation technique. A total of 3 g of PLGA was dissolved in 30 mL of dichloromethane. In addition, 0.2 g of melatonin powder was dissolved in 200 μL of DMSO and 200 μL of methanol. A total of 2 mg of TRITC was dissolved in 200 μL of DMSO to methanol (1 : 1) solution. The TRITC solution was emulsified with the PLGA solution. The mixture was dropped into 50 mL of 2% (w/v) aqueous PVA using a syringe with a 23-gauge needle and mechanically stirred for 3 h at 450 rpm. After lyophilization, NPs were dissolved in distilled water to a concentration of 10 mg mL$^{-1}$.
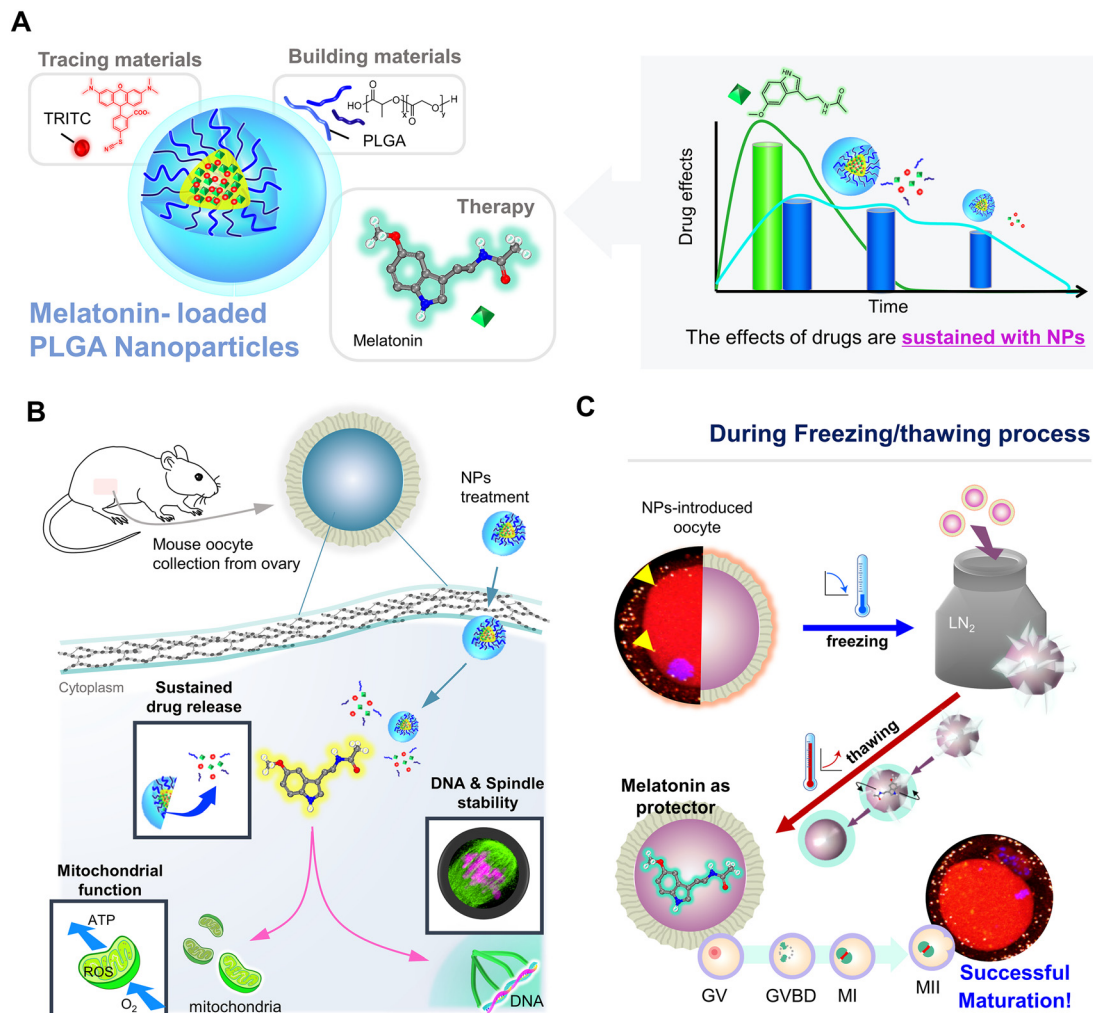
### 2.3 Characterization of melatonin-loaded NPs

The size and zeta potential of melatonin/TRITC-loaded PLGA NPs were measured using a Zetasizer Nano ZS instrument (Malvern, Southborough, MA, USA). The morphologies of NPs were observed using a SEM (Hitachi, Tokyo, Japan). Fluorescence was measured using a Spectramax iD5 microplate reader (Molecular Devices, CA, USA). The loaded components were confirmed by FT-IR analysis. Spectra at a wavelength of 650–4000 cm$^{-1}$ were determined using an IRTracer-100 spectrometer (Shimadzu Co., Kyoto, Japan). The spectrum of air was used as a background. Sample spectra were recorded at RT at a resolution of 4 cm$^{-1}$. Each measurement was performed 64 times.

### 2.4 Drug loading and encapsulation efficiencies

Lyophilized melatonin/TRITC-loaded PLGA nanoparticles (10 mg) were dissolved in 1 mL of methanol and measured

**Scheme 1** Schematic diagram of melatonin delivery *via* NPs and their functions. (A) Components of NPs. (B) Delivery of melatonin to oocytes and its effect (C) Melatonin-loaded NPs relieve freezing/thawing-induced damage during vitrification to successfully induce maturation.

using a spectrophotometer at 278 nm. The melatonin concentration was calculated using a standard melatonin UV calibration curve.

The drug loading and encapsulation efficiency were calculated using the following equation:

$$\text{Encapsulation efficiency}(\%) = \\ (\text{Amount of melatonin released from the NPs}/ \\ \text{Amount of initial melatonin used}) \times 100\%$$

$$\text{Drug loading}(\%) = \\ (\text{Amount of melatonin released from the NPs}/\text{Amount of NPs}) \\ \times 100\%$$

### 2.5 Analysis of the release of melatonin and TRITC from NPs *in vitro*

To analyze the release of melatonin and TRITC from PLGA NPs *in vitro*, lyophilized NPs (10 mg) were dissolved in 1 mL of PBS

(pH 7.4) or distilled water and incubated at 37 °C or RT. Supernatants were collected at 0–24 h, replaced with an equal volume of fresh solution, and analyzed using a Spectramax iD5 instrument (Molecular Devices). Melatonin was detected at 314 nm, and TRITC was detected at an emission wavelength of 580 nm. The melatonin and TRITC contents were determined using standard calibration curves drawn using a series of diluted samples.

### 2.6 Animals

All mice used in experiments were 4-week-old ICR mice purchased from Orient Bio (Seongnam-si, Republic of Korea). They were housed under temperature- and light-controlled conditions with lights on for 12 h daily. The care of mice and the experimental and surgical procedures were performed in accordance with the Guide for the Care and Use of Laboratory Animals and were approved by the Institutional Agricultural Animal Care and Use Committee of CHA University (approval numbers IACUC200167 and IACUC210158).

## 2.7 Collection and treatment of mouse oocytes

Ovaries were removed from 4-week-old female ICR mice at 46–48 h after intraperitoneal injection of 7.5 IU pregnant mare serum gonadotropin (DAESUNG, Uiwang-si, Republic of Korea). They were transferred to M2 medium containing IBMX in a 35 mm dish. IBMX was used to prevent oocyte maturation during oocyte collection. Germinal vesicle (GV)-stage oocytes were obtained by puncturing ovaries using a 1 mL syringe with a 26-gauge needle. They were mechanically denuded using thin glass capillaries to remove surrounding cumulus cell layers. Oocytes were divided into control (nontreated) and experimental groups. Treatment was performed in serum-free DMEM-high supplemented with 0.5% IBMX. DNA damage was induced by treatment with 50 μM ETP, which is a topoisomerase inhibitor II, in a humidified 5% $CO_2$ incubator at 37 °C for 1 h. ETP-treated samples were washed three times with fresh medium and treated with melatonin or melatonin-loaded NPs. Samples were treated with melatonin at a concentration of 1.25 mM (corresponding to the melatonin concentration embedded in PLGA NPs) or 0.416 mM (in the case of multidrug treatment, equivalent to 1/3 of 1.25 mM) or with 10 μg of melatonin-PLGA NPs. They were treated three times for 1 h in the case of multidrug treatment or for 3 h otherwise. After treatment, the samples were used for further experiments or subjected to in vitro maturation.

## 2.8 In vitro maturation

GV-stage oocytes in each experimental group were transferred to M16 medium containing 1% BSA and 1% antibiotics. In vitro maturation was performed in a humidified 5% $CO_2$ incubator at 37 °C for 16 h. Upon maturation, GV-stage oocytes go through GV breakdown (GVBD), metaphase of meiosis I (MI), and MII stages. The maturation ratio was calculated as the ratio of mature oocytes to total oocytes.

## 2.9 Vitrification and thawing of mouse oocytes

Oocyte vitrification and thawing were performed according to the methods described in ref. 49 and 50 with minor modifications. Briefly, the oocytes were placed in equilibration solution (7.5% ethylene glycol (EG), 7.5% DMSO, 20% BSA in M2 medium) for 3 min and then transferred to vitrification solution (15% EG, 15% DMSO, 0.5 M Sucrose in M2 medium) for 60 s. Finally, the oocytes were transferred to a cryovial and then immediately plunged into LN2 and stored in the LN2 tank for 0.25 hours or 0.5 hours. For thawing, the oocytes were retrieved from the cryovial and then transferred into the thawing solution (0.5 M sucrose, 0.25 M sucrose, 0.125 M sucrose in M2 medium). Viable oocytes were transferred to M16 medium for in vitro maturation.

## 2.10 Comet assay

Experiments were performed according to the manufacturer's manual with slight modifications. Briefly, groups of 25–30 oocytes were washed in 1X PBS (without calcium and magnesium) and then mixed with LMA. 50 μl of LMA solution was added to Comet slides and then incubated for 30 min at 4 °C for gelation. Next, the slides were immersed in lysis solution for 60 min at 4 °C followed by alkaline unwinding solution for 1 h at 4 °C in the dark. Electrophoresis was performed at 21 V for 30 min maintaining a cool status. Washing with $dH_2O$ for 5 min twice and 70% ethanol for 5 min. Samples were dried at 37 °C for 10–15 min. Nuclei staining was performed with Midori Green solution for 30 min, then briefly washed with water, and fully dried at 37 °C. The tail length was measured using a confocal laser microscopy imaging and analyzed using CASP software (CASP ver. 1.2.3, Krzysztof Konca; casplab.com).

## 2.11 Mitochondrial distribution analysis and membrane potential measurement in oocytes

MitoTracker was used to stain mitochondria for mitochondrial distribution analysis. TMRE was used to measure the mitochondrial membrane potential. MitoTracker™ Green FM (M7514) was dissolved in DMSO to prepare a 1 mM stock solution. TMRE (T669; Invitrogen, MA, USA) was dissolved in DMSO to prepare a 500 μM stock solution. Both solutions were stored at −20 °C until use. They were added to growth medium (M16 medium supplemented with 1% BSA and antibiotics) at a final concentration of 1 μM and the samples were incubated for 20 min in a humidified 5% $CO_2$ incubator at 37 °C. The stained oocytes were imaged using an Olympus FV3000 confocal laser scanning microscope. The mitochondrial distribution and membrane potential were analyzed using ImageJ software.

## 2.12 Measurement of the intracellular ATP content

Intracellular ATP contents were measured using an ATP Determination Kit (Invitrogen) according to the manufacturer's protocol with slight modifications. Briefly, fresh oocytes (30 oocytes per group) were collected in an Eppendorf tube and supplemented with 100 μL of lysis buffer. After centrifugation for 10 min at 13 000 rpm at 4 °C, the supernatant was used in the experiment. The bioluminescence of each sample was measured using a Spectramax iD5 microplate reader (Molecular Devices). ATP contents were calculated using a standard curve drawn using a gradient of ATP concentrations ranging from 0 to 100 nM. The intracellular ATP content of each oocyte was calculated.

## 2.13 Measurement of the intracellular ROS level

5-(and-6)-Chloromethyl-2′,7′-dichlorodihydrofluorescein diacetate, acetyl ester (CM-H2DCFDA) (C6827, Invitrogen), is a cell-permeant dye that diffuses into cells and is used to measure intracellular ROS levels. CM-H2DCFDA was diluted with DMSO to generate a 1 mM stock solution. Oocytes were incubated in M16 medium containing 500 μM CM-H2DCFDA for 20 min in a humidified 5% $CO_2$ incubator at 37 °C. After washing with PBS, oocytes were transferred to a 35 mm confocal dish, and then fluorescence was detected using an Olympus FV3000 confocal laser scanning microscope with excitation and emission wavelengths of 485 and 535 nm, respectively.

### 2.14 Immunofluorescence staining

After treatment, the oocytes were washed three times in PBS containing 0.1% PVA (0.1% PVA-PBS), fixed in 4% paraformaldehyde for 30 min at RT, washed three times, and permeabilized in 0.1% PVA-PBS containing 0.2% Triton X-100 for 30 min. Nuclei were stained with DAPI (4′,6-diamidino-2-phenylindole) (1 : 500 dilution; Thermo Fisher Scientific, #62248) for 5 min at RT. If necessary, membrane staining was performed using Alexa Fluor™ 647 phalloidin (A22287, Invitrogen) diluted 1 : 100 in PBS for 5 min at RT. Immunofluorescence imaging of oocytes was performed using an Olympus FV3000 confocal laser scanning microscope. The following antibodies were used: anti-alpha tubulin (1/100, #ab15246, Abcam), anti-γH2A.X (phospho Ser139) (3F2) (1/1000, #ab22551, Abcam), anti-phospho-histone H2A.X (Ser139) (1/1000, #2577, Cell Signaling), anti-RAD51 (1/500, #ab63801, Abcam), and anti-DNA-PKCs (E6U3A) (1/100, #38168, Cell Signaling).

### 2.15 ELISA of the intracellular melatonin concentrate

The intracellular melatonin concentration was measured using a mouse melatonin ELISA kit (#LS-F25779, LSBio) based on a competitive enzyme immunoassay according to the manufacturer's manual. In brief, 30 oocytes per group were lysed in hypotonic lysis buffer (5 mM Tris, 20 mM EDTA, and 0.5% Triton X-100, adjusted to pH 8.0) and centrifuged (10 000$g$ for 30 min at 4 °C). The supernatants were stored at −20 °C until all samples were collected. The optical density of each well was immediately determined using a microplate reader set to a wavelength of 450 nm. The intracellular melatonin concentration was calculated from a standard curve of melatonin.

### 2.16 Statistical analysis

Data are representative results or the mean ± standard deviation (s.d.) of at least three independent experiments. Statistical analyses were performed using Student's $t$-test. ns: $p > 0.05$, $*p < 0.05$, $**p < 0.01$, and $***p < 0.001$.

## 3. Results and discussion

### 3.1 Characterization of NPs and their application to mouse oocytes

Biodegradable PLGA NPs were simultaneously loaded with melatonin and TRITC as a drug and tracer, respectively (Fig. 1A). Successful delivery of NPs into oocytes was tracked using the fluorescent probe TRITC. The size of these NPs was measured by dynamic light scattering (DLS). The average diameter of NPs was ~198 nm, which is optimal for the delivery of NPs as a drug delivery system, and their zeta potential was about −3.31 mV (Fig. S1†). The shape and size distribution of NPs were assessed by scanning electron microscopy (SEM). They had a spheroid shape and an even size distribution (Fig. 1B). To confirm that melatonin and TRITC were appropriately loaded inside NPs, fluorescence detection and Fourier transform infrared spectroscopy (FT-IR) analyses were per-

formed. Internalization of TRITC was confirmed by the fluorescence peak at 580 nm, which is its emission wavelength (Fig. 1C and Fig. S2A†). To check the stability of NPs, they were dispersed in phosphate-buffered saline (PBS, pH 7.4), and the degradation of NPs and the cumulative release of melatonin and TRITC were analysed over time at room temperature (RT, 25 °C) or 37 °C (Fig. 1D, a, b and Fig. S3†). The supernatant was collected at each time point, and the melatonin and TRITC contents were determined by measuring absorbance at 314 nm and emission at 580 nm, respectively. The release of melatonin and TRITC increased over time and was higher at 37 °C than at 25 °C and about 50% of the loaded contents were released after 24 h.

Next, the spectra of melatonin, PLGA NPs, TRITC-loaded PLGA NPs, and melatonin/TRITC-loaded PLGA NPs were compared by FT-IR analysis to confirm the presence of melatonin and TRITC according to the detection of specific functional groups (Fig. 1E). Representative peaks of melatonin (1650 and 1200 cm$^{-1}$) were observed with melatonin/TRITC-loaded PLGA NPs (blue arrows). In addition, a peak at 1450 cm$^{-1}$, which was observed with TRITC-loaded PLGA NPs but not with unloaded PLGA NPs, was also observed with melatonin/TRITC-loaded PLGA NPs (red arrows). These results prove that melatonin and TRITC were loaded into PLGA NPs. The encapsulation efficiency of the synthesized nanoparticles was found to be 42% and the drug loading (%) was about 3.82%. Next, we tested whether NPs were effectively delivered into oocytes. Oocytes were treated with melatonin/TRITC-loaded PLGA NPs for 2 h and then imaged using a confocal laser scanning microscope (Fig. 1F). The fluorescence intensity of TRITC increased with the volume of NPs (Fig. S2B†). Fluorescence profiling after membrane staining revealed that NPs were effectively introduced into the oocyte cytoplasm (yellow arrows). Unlike drugs delivered by simple diffusion, drugs loaded on nanoparticles are delivered into cells through endocytosis. Melatonin-loaded NPs are delivered into cells through endocytosis and then degraded by lysosomes. So, internalized NPs were confirmed by lysosomal staining and the colocalized region of the lysosomes and NPs indicates the effective internalization of NPs (Fig S4†). These results show that the prepared NPs can be successfully delivered into oocytes as drug carriers.

### 3.2 Melatonin-loaded NPs effectively repair ETP-induced DNA damage

Exposure of cells to a chemical agent such as etoposide (ETP, a DNA topoisomerase inhibitor) or carcinogens causes DNA damage. When DNA damage (in case, DNA double strand break (DSB)) occurs, an early cellular response to DSB is observed, which occurs due to the rapid phosphorylation of H2A.X, the minor histone H2A variant, at Ser-139 to produce γH2A.X. ETP-treated oocytes were then treated with NPs and NP bearing oocytes were evaluated for DNA damage recovery abilities (Fig. 2A). To investigate whether melatonin treatment could help DNA damage repair and to compare the effects of treatment with melatonin and melatonin-loaded NPs, oocytes were divided into a control group not treated with ETP and an
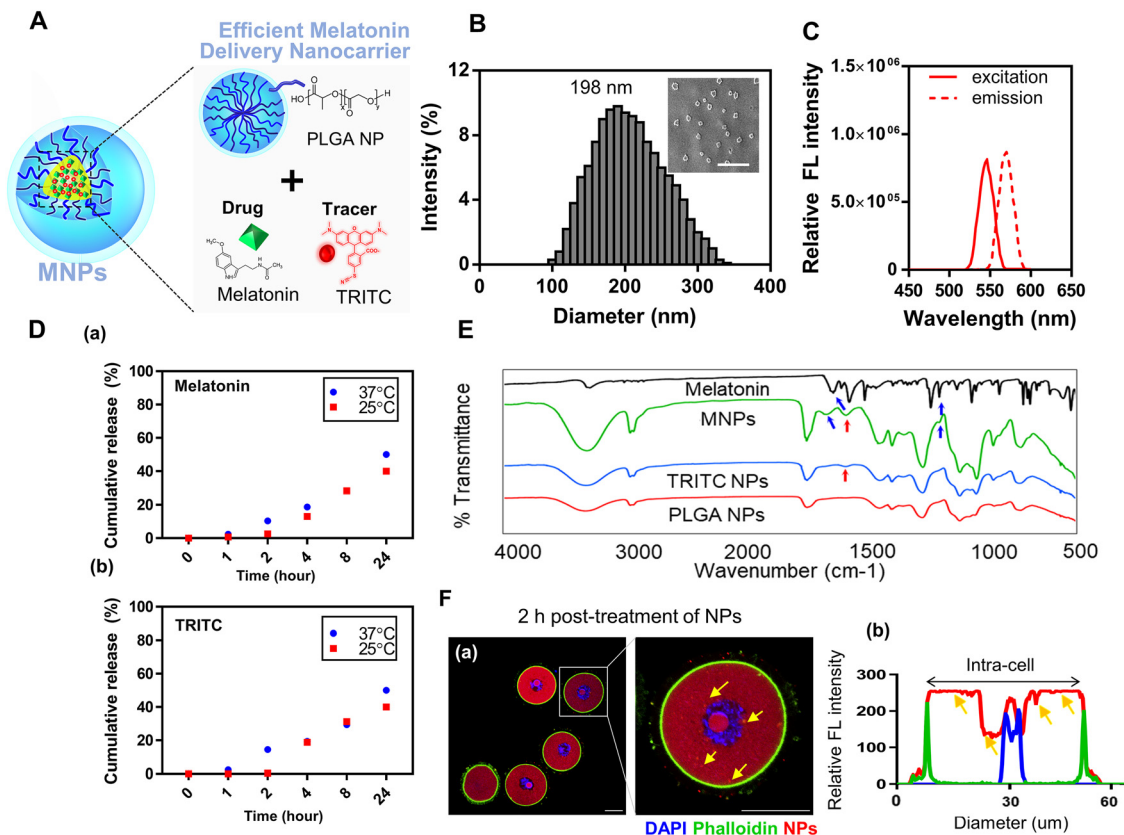
**Fig. 1** Characterization of NPs and their application to mouse oocytes. (A) A brief schematic illustration. (B) Size and distribution of NPs determined by DLS and SEM. Scale bar: 500 nm. (C) Fluorescence properties of NPs. (D) (a) Cumulative release profiles of melatonin loaded in NPs by measuring absorbance until 24 hours. (b) Cumulative release profiles of TRITC loaded in NPs by measuring fluorescence. (E) Comparison of functional groups by FT-IR analysis. Blue arrows represent melatonin-specific peaks and red arrows are TRITC-specific. (F) (a) Confocal laser scanning microscopy (CLSM) images of NP-treated oocytes. DAPI (blue), membrane (green), and NPs (red). Scale bar: 50 μm. (b) Fluorescence intensity profiles. Yellow arrows indicate internalized NPs.

experimental group treated with ETP. We tested the effects of various ETP concentrations on *in vitro* maturation and the DNA damage degree, because a self-healing effect may occur during the maturation process after ETP treatment, and we selected an optimized concentration of 50 μM (Fig. S5†). ETP-treated oocytes were divided into DS (1.25 mM for 3 h), DM (three times with 0.416 mM for 1 h each time), NP, and untreated groups (ETP).

Phosphorylation of H2A.X tends to increase proportionally with DNA damage, and regulation of γH2A.X is essential for DNA repair.[51] The γH2A.X level was analyzed by immunofluorescence after ETP treatment for 1 h. In the ETP-treated group, γH2A.X foci, which represented DSBs in a 1 : 1 manner, appeared sporadically in the nuclear region, and the number of these foci was significantly higher than that in the control group (Fig. 2B). To evaluate the degree of DSB repair upon melatonin treatment, the number of γH2A.X foci was counted upon treatment with melatonin once or thrice or with melatonin-loaded NPs. The number of γH2A.X foci was significantly lower in melatonin-treated groups than in the ETP-treated group, but did not significantly differ between the DS, DM, and NP groups (Fig. 2C).

Next, we performed a comet assay to examine the DNA damage degree (Fig. 2D). When DNA damage or fragmentation occurs, longer tails appear on electrophoresis. The tendency of DNA damage was similar to that of rH2A.X levels. These data suggest that the delivery of melatonin effectively repairs ETP-induced DNA damage.

### 3.3 The structural and functional state of mitochondria is stabilized by NPs

?Etoposide is an anticancer drug that causes DNA damage by inhibiting topoisomerase II, but it is also known to cause mitochondrial dysfunction and cellular senescence.[52] As melatonin is well-known to act as a ROS scavenger, we therefore evaluated the effect of melatonin treatment on mitochondrial activity in ETP-induced damaged oocytes.

When mitochondria were indirectly damaged by ETP treatment on oocytes, we evaluated the structural, distributional, and functional effects of melatonin treatment on mitochondria. Mitochondrial distribution was measured using MitoTracker staining (Fig. 3A). Mitochondria were uniformly dispersed throughout the cytoplasm of control oocytes, whereas many aggregated mitochondria were observed in ETP-
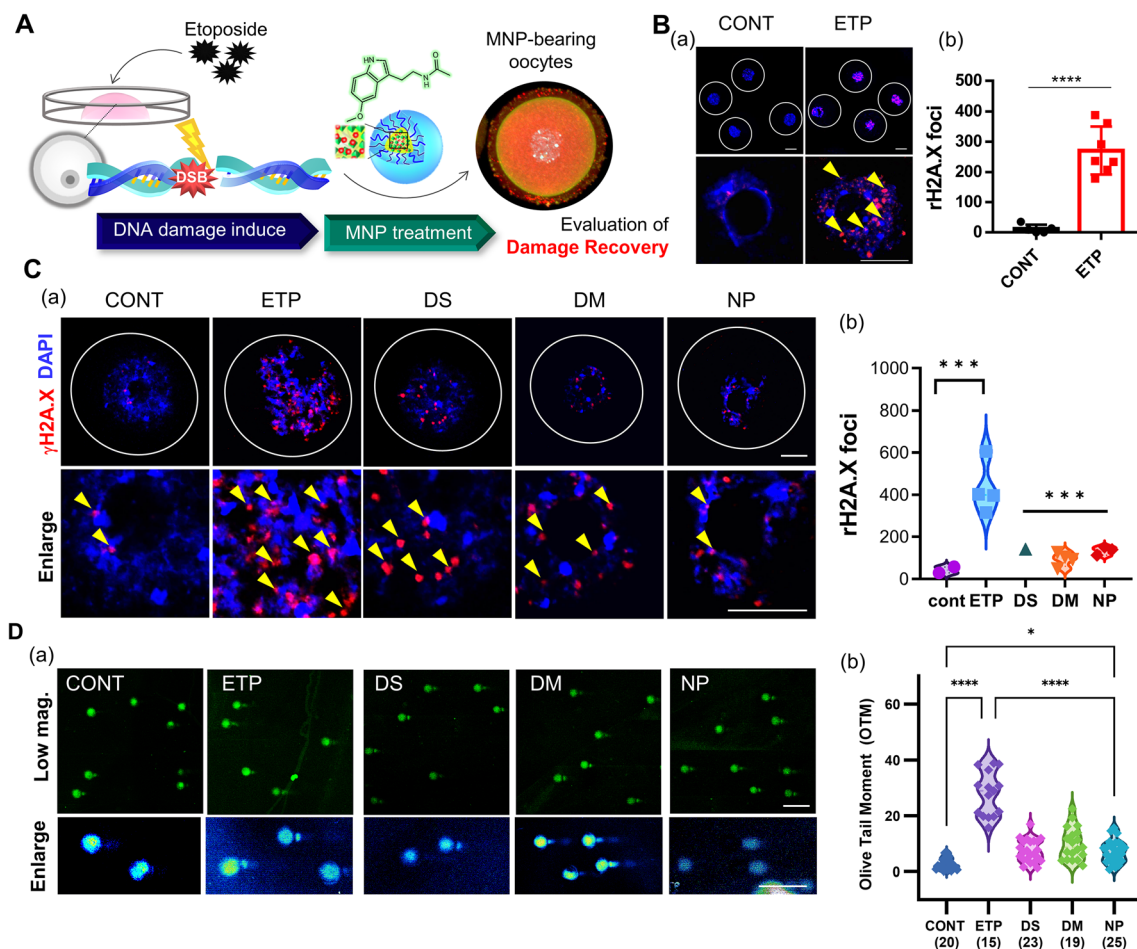
**Fig. 2** Effects of melatonin-loaded NPs on DNA damage in mouse oocytes. (A) A brief schematic illustration of inducement of DNA damage and evaluation of degrees after NP treatment. (B) Immunofluorescence analysis of γH2A.X (red) foci in oocytes treated with 50 μM ETP for 1 h. DAPI (blue) and yellow arrows indicate DSB. (C) (a) DNA damage measured by γH2A.X foci using CLSM in ETP-treated oocytes after melatonin treatment. Scale bar: 20 μm. (b) Quantitative analysis of γH2A.X foci count per cell. (D) (a) DNA damage measured by the comet assay in ETP-treated and melatonin-treated oocytes. Scale bar: 100 μm. (b) Olive tail moments were measured by the fluorescence intensity of the tail and nucleus using CASP software. Parentheses indicate the number of oocytes used for measurement. All experiments were performed with at least 3 replicates.

treated oocytes. The distribution of mitochondria was assessed in ETP-exposed oocytes treated with melatonin or melatonin-loaded NPs. Some mitochondrial aggregates remained upon treatment with melatonin, but the distribution of mitochondria was similar to that in control oocytes upon treatment with melatonin-loaded NPs. For quantitative analysis, the fluorescence signal of mitochondria was simplified and converted into a particle shape, and then the particle number and size in the region of interest were determined as the mitochondrial number and size, respectively. The number of mitochondria was significantly lower and the size of mitochondria was larger in ETP-treated oocytes than in control oocytes. This demonstrates that the formation of aggregated mitochondria was increased in ETP-treated oocytes. However, in oocytes treated with melatonin and melatonin-loaded NPs, the number of mitochondria was lower than that in control oocytes but higher than that in ETP-treated oocytes. In addition, the number of mitochondria was higher in oocytes treated with

melatonin-loaded NPs than in those treated with melatonin (Fig. S6†). These results showed that mitochondrial morphology and homogeneity in damaged oocytes are ameliorated more by sustained release of melatonin from NPs than by treatment with melatonin alone.

Next, we analyzed mitochondrial function. First, a tetramethylrhodamine ethyl ester (TMRE) assay was performed to analyze changes in the mitochondrial membrane potential (Fig. 3B, upper panel). TMRE is a cell-permeant, positively charged, red-orange dye that readily accumulates in active mitochondria due to its relative negative charge.

Differences in the mitochondrial membrane potential can be indirectly determined by comparing TMRE fluorescence intensities. The fluorescence intensity of TMRE, which was quantified after imaging with a confocal laser microscope, did not differ between the groups (Fig. 3C). Second, the level of ROS was evaluated using CM-H2DCFDA, which reacts with intracellular ROS and generates a green signal (Fig. 3B, lower
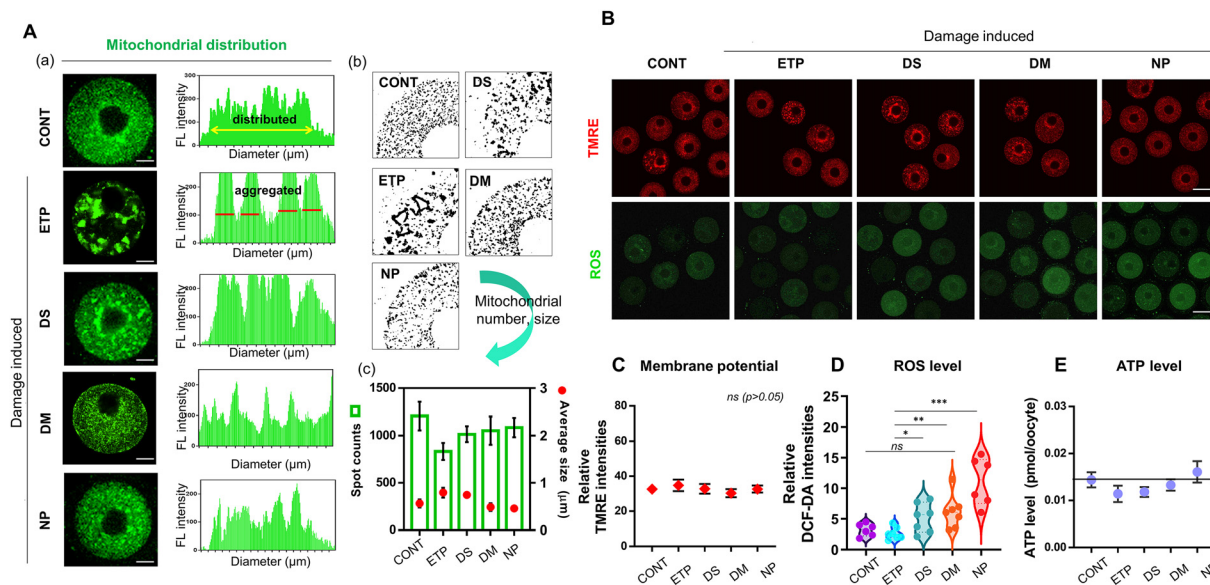
**Fig. 3** Effect of melatonin on the mitochondrial distribution and function in damaged mouse oocytes. (A) (a) Intracellular mitochondrial distribution determined by MitoTracker staining. (b) Postprocessing analysis using Image J. (c) Bar represents the mean value ± s.d. of the mitochondrial number and round symbols indicate the mitochondrial size. (B) CLSM images of TMRE staining (red, membrane potential) or CM-H2DCFDA staining (green, ROS level). Scale bar: 50 μm. Quantification of (C) mitochondrial membrane potential, (D) ROS level, and (E) ATP level (pmol/oocyte). All experiments were performed with at least 3 biological replicates.

panel). The ROS level was lower in ETP-treated oocytes than in control oocytes. Interestingly, the average ROS level was higher in the melatonin treated group than in the control group (average values are 5.19 (±2.18), 6.14 (±2.53), and 11.1(±3.60) in the DS, DM, and NP groups, respectively). ROS are generated when mitochondria are activated to produce ATP, the energy required for cell metabolism. Therefore, these results show that mitochondrial damage is induced in ETP-treated oocytes, and that mitochondrial function is improved by treatment with melatonin and particularly with melatonin-loaded NPs (Fig. 3D). Similarly, we investigated intracellular ATP levels to assess the extent of mitochondrial damage repair (Fig. 3E). The intracellular ATP levels measured using a luminometer showed a similar tendency to the ROS levels. The intracellular ATP level was ~0.78 times lower in the ETP-treated group than that in the control group and was 1.12 and 1.42 times higher in the NP group than in the control and ETP-treated groups, respectively. The increase in the ATP level suggests that mitochondrial function was somewhat restored in the NP group.

### 3.4 Delivery of melatonin *via* NPs enhances meiotic maturation of deteriorated oocytes

We investigated how the sustained release mode of melatonin when delivered in nanoparticle form affects the maturation process *in vitro*. In this method, melatonin delivery has a longer lasting time effect on oocyte maturation than that delivered by simple diffusion due to an increase in the half-life (Fig. 4A).

An enzyme-linked immunosorbent assay (ELISA) was performed to investigate whether melatonin was delivered into

oocytes and its concentration (Fig. 4B). The intracellular melatonin concentration was higher in oocytes treated with melatonin than in control and etoposide (ETP)-treated oocytes. In addition, the concentration of melatonin was higher in oocytes treated with melatonin multiple times (multiple drug treatments, DM group) and melatonin-loaded NPs (NP group) than in oocytes treated with melatonin once (single treatment, DS group). These results confirmed that melatonin can be successfully delivered into oocytes, and the concentration of melatonin in oocytes was increased upon treatment with melatonin-loaded NPs due to sustained drug release.

We investigated the *in vitro* maturation of treated oocytes. Fig. 4D shows the result of *in vitro* maturation after each treatment was performed on the damage-induced oocyte. As shown in the scheme of Fig. 4A, the maturation process of an oocyte is largely divided into 4 stages. First, the initial oocyte exists in the germinal vesicle (GV) state, and as meiosis proceeds, it enters the germinal vesicle breakdown (GVBD) stage, metaphase I-arrest (MI) stage, and finally reaches the metaphase II-arrest (MII) stage. The blue arrow indicates the MII oocyte, and the maturation rate is shown in Fig. 4E. After *in vitro* maturation induced for 18 h, the maturation rate was ~35% in the ETP-treated group, which was more than one-half lower than that in the control group (~80%). On the other hand, the maturation rate was increased in the melatonin-treated groups after damage induction. It was higher in the DM group than in the DS group and was similar in NP and DM groups (42%, 59%, and 58% in the DS, DM, and NP groups, respectively) (Fig. 4D, E and Table S1†). This confirmed that melatonin treatment improved the maturation of damaged oocytes.
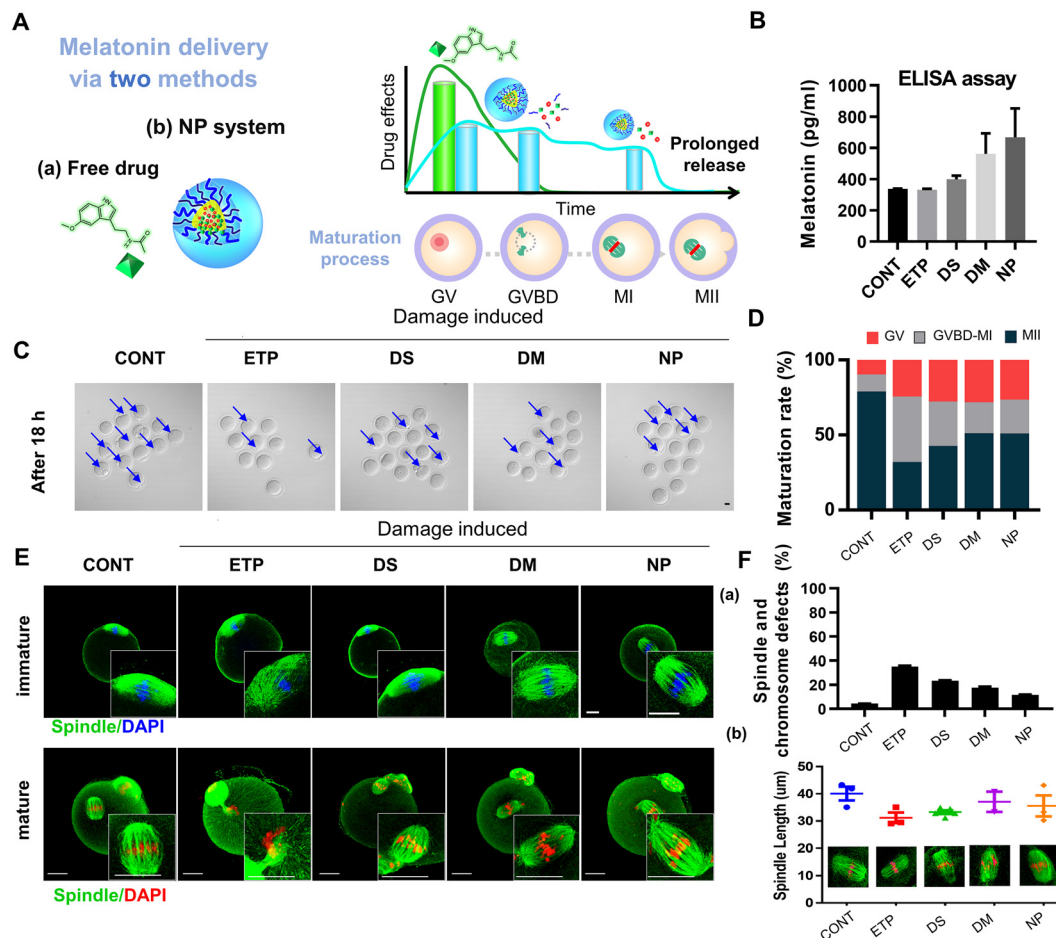
**Fig. 4** Effect of melatonin on the meiotic maturation of damaged mouse oocytes (A) Schematic illustration of melatonin delivery using two methods: the use of (i) free drug form and (ii) NP system and *in vitro* maturation was performed. (B) Intracellular melatonin concentration measured using an ELISA. The experiment was performed in duplicate. Bar represents the mean value $\pm$ s.d. (C) CLSM images of oocytes ($n > 10$) after each treatment. Blue arrows indicate mature oocytes. (D) Maturation rate. Data were pooled from at least 5 biological replicates. Detailed data related to (D) are presented in Table S1 (ESI†). (E) Representative CLSM image to analyze spindle stability. Spindle (green) and DAPI (blue or red). (F) (a) Quantitative analysis of spindle defects. Experiments were performed in duplicate and the bar represents the mean value $\pm$ s.d. (b) Quantitative analysis of the meiotic spindle length in mature oocytes. Individual values and medians are shown. ($n \geq 5$). Precise *p* values are presented in Table S2 (ESI†). All CLSM images show a scale bar of 25 µm.

Next, a spindle morphology was analyzed by immunofluorescence to determine whether the effect of melatonin on maturation was due to the alteration of spindle stability during meiosis. After inducing maturation to the metaphase of the meiosis II (MII) stage, the spindle morphology of immature oocytes was analyzed (Fig. 4F). Normal spindles had a barrel shape, while abnormal spindles had a fragmented or asymmetric shape. The percentage of oocytes with abnormal spindles was higher in the ETP-treated group than in the control group (35.3% and 4.3%, respectively). And the abnormalities decreased in DS, DM, and NP groups compared to the ETP-treated group (23.5%, 17.6%, and 11.8% in the DS, DM, and NP groups, respectively) (Fig. 4G, a). Oocytes undergo a second meiotic division to reach the MII stage where they have a polar body. The spindle length in the oocyte was measured (Fig. 4G, b). It was 40.09 µm in the control group; was slightly shorter in

the ETP-treated group at 31.2 µm; and was 33.3, 37.10, and 35.6 µm in the DS, DM, and NP groups, respectively.

These results demonstrate that if damaged oocytes are not treated with melatonin, the recovery rate of the damaged spindle decreases, and meiosis does not resume, whereas melatonin treatment reduces spindle abnormalities and improves the maturation rate. Moreover, spindles are slightly shortened or disorganized in damaged oocytes, but these abnormalities are mitigated by treatment with melatonin or melatonin-loaded NPs.

### 3.5 Internalization of NPs increases cryotolerance to damage during vitrification

This effect of melatonin was examined during cryopreservation of the oocytes (Fig. 5). After inducing damage to the oocytes in the GV state with ETP, the NPs were delivered into oocytes,
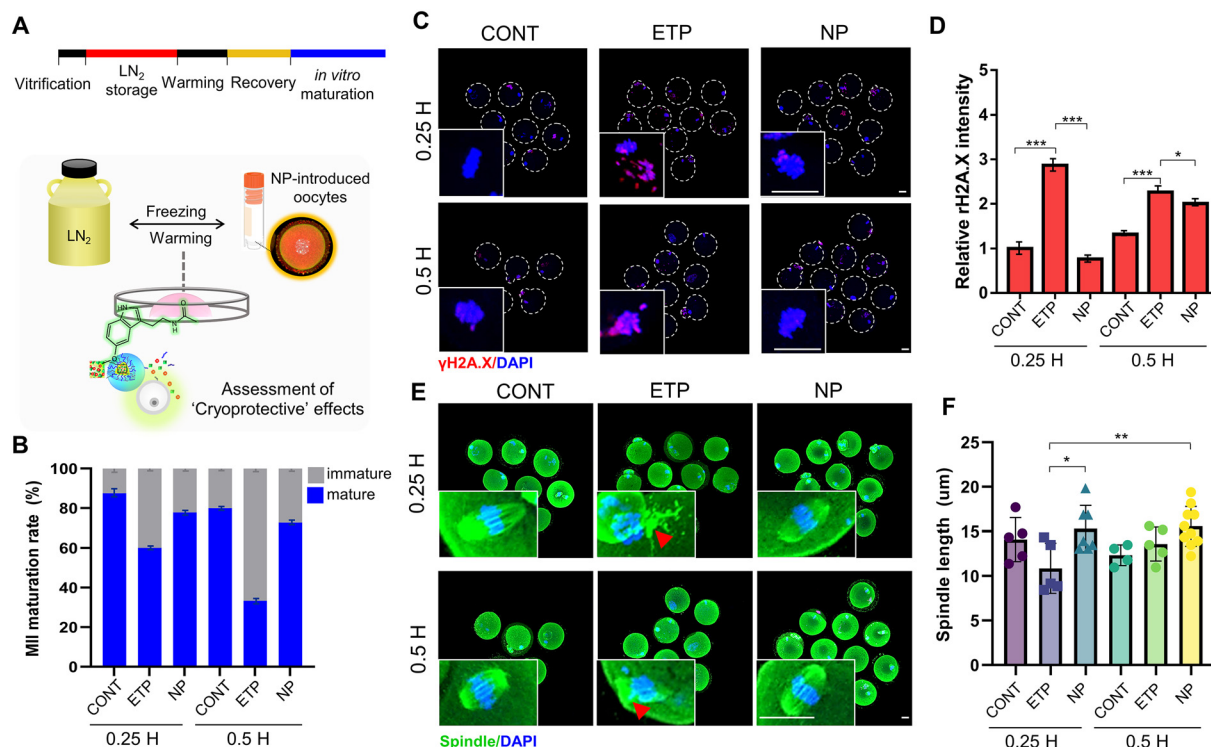
**Fig. 5** Verification of the cryoprotective effect of NPs in vitrified-warmed mouse oocytes. (A) Vitrification and thawing process of NP-treated oocytes. (B) Maturation rate after vitrification and thawing. Oocytes were treated with 50 μM ETP for 1 h and then with NPs for 2 h. LN2 storage was performed for 0.25 hours and 0.5 hours. (C) Evaluation of DNA damage *via* the γH2A.X level by CLSM images. DAPI (blue) and rH2A.X (red). Scale bar: 20 μm. (D) Quantification of the relative rH2A.X intensity. (E) Spindle morphology was confirmed by immunofluorescence. DAPI (blue), spindle (green) and the red arrowhead indicates abnormal spindles. Scale bar: 20 μm. (F) Spindle length was measured using CLSM images and ImageJ software. Individual values and medians are shown ($n \geq 5$).

transferred sequentially to equilibrium solution and vitrification solution, and then placed in liquid nitrogen solution for vitrification. After the thawing process (recovery time of 1 h), the oocytes were observed to undergo *in vitro* maturation (Fig. 5A). Since long-term storage (about 1 h) induced severe maturation inhibition (Fig. S7†), LN2 storage times were set to 15 and 30 minutes and are represented by 0.25 h and 0.5 h, respectively. After thawing, the maturation rate of oocyte conversion to MII in the GV state decreased in the ETP-treated group (40–60%), whereas the NP-treated oocyte group had a similar level to the control group (about 70–80%) (Fig. 5B). The rH2A.X level, the degree of DNA damage in the oocytes, increased in the ETP-treated group, and decreased compared to the ETP in the NP-treated group after ETP treatment (Fig. 5C). Fig. 5D shows the comparison result of the relative values after quantifying the rH2A.X signal in oocytes marked with a dashed circle and setting the control group value to 1.

Furthermore, the spindles of the MII stage of the oocytes, the cytoskeletal structure of cells that forms during cell division, were observed. The ETP-treated oocytes showed a lot of abnormal spindle shapes (red arrowheads), and the spindle length was shortened, whereas the NP-treated oocytes showed a normal spindle shape and a significantly longer spindle length compared to the ETP-treated group (Fig. 5E and F). This

result indicates that the shape and length of spindles in oocytes treated with NPs were almost similar to those of the control group. This pattern was observed to have higher normality at 0.25 h than at 0.5 h. These results show that melatonin is capable of recovering DNA from damaged oocytes in the freezing process, and this effect was supposed to be better in the short-term (0.25 h) than in the long-term (0.5 h). For this reason, the delivery of melatonin into the cytoplasm of oocytes has a better effect than the injection of melatonin into oocytes in the media.

## 4. Conclusions

In this study, we found that biodegradable PLGA NPs loaded with both melatonin (drug) and TRITC (tracer) repaired ETP-induced DNA and mitochondrial damage in oocytes. The effects of melatonin (one or three doses) and melatonin-loaded NPs on ETP-induced DNA and mitochondrial damage in oocytes were determined. Melatonin not only facilitates the repair of DSBs but also improves mitochondrial distribution and function. Compared with melatonin treatment alone, sustained release of melatonin by NPs greatly improved DNA repair and mitochondrial stability in oocytes. The delivery of

melatonin by NPs efficiently improves the quality of damaged oocytes by repairing DNA damage, improving mitochondrial distribution, and facilitating the maturation process. In addition, it was confirmed that when oocytes containing NPs were vitrified/thawed, internal melatonin showed a cryopreservation effect during the thawing process to alleviate cell damage.

## Author contributions

Sujin Lee: conceptualization, investigation, writing – original draft, data curation, formal analysis, and validation. Hye Jin Kim: investigation and visualization. Hui Bang Cho: methodology and visualization. Hye-Ryoung Kim: formal analysis. Sujeong Lee: methodology. Ji-In Park: formal analysis. Keun-Hong Park: conceptualization, writing – review & editing, project administration and supervision.

## Conflicts of interest

There are no conflicts to declare.

## Acknowledgements

## References

1 D. T. Armstrong, X. Zhang, B. C. Vanderhyden and F. Khamsi, *Ann. N. Y. Acad. Sci.*, 1991, **626**, 137–158.

2 E. C. Coucouvanis, S. W. Sherwood, C. Carswell-Crumpton, E. G. Spack and P. P. Jones, *Exp. Cell Res.*, 1993, **209**, 238–247.

3 Y. Matsui, *Int. J. Dev. Biol.*, 1998, **42**, 1037–1042.

4 P. Guérin, S. E. Mouatassim and Y. Ménézo, *Hum. Reprod. Update*, 2001, **7**, 175–189.

5 J.-M. Cheng, J. Li, J.-X. Tang, S.-R. Chen, S.-L. Deng, C. Jin, Y. Zhang, X.-X. Wang, C.-X. Zhou and Y.-X. Liu, *Cell Cycle*, 2016, **15**, 2454–2463.

6 R.-Y. Yuan, F. Wang, S. Li, J.-Y. Ma, L. Guo, X.-L. Li, H.-J. Zhu, X. Feng, Q.-N. Li, Q. Zhou, Z.-B. Lin, H. Schatten and X.-H. Ou, *J. Assist. Reprod. Genet.*, 2021, **38**, 1373–1385.

7 S. Prasad, M. Tiwari, A. N. Pandey, T. G. Shrivastav and S. K. Chaube, *J. Biomed. Sci.*, 2016, **23**, 1656–1661.

8 E. ElInati, A. P. Zielinska, A. McCarthy, N. Kubikova, V. Maciulyte, S. Mahadevaiah, M. N. Sangrithi, O. Ojarikre, D. Wells, K. K. Niakan, M. Schuh and J. M. A. Turner, *Nat. Commun.*, 2020, **11**, 2598.

9 W. P. Roos and B. Kaina, *Trends Mol. Med.*, 2006, **12**, 440–450.

10 J. B. Kerr, K. J. Hutt, E. M. Michalak, M. Cook, C. J. Vandenberg, S. H. Liew, P. Bouillet, A. Mills, C. L. Scott, J. K. Findlay and A. Strasser, *Mol. Cell*, 2012, **48**, 343–352.

11 J. Carroll and P. Marangos, *Front. Genet.*, 2013, **4**(117), DOI: **10.3389/fgene.2013.00117**.

12 A. L. Winship, J. M. Stringer, S. H. Liew and K. J. Hutt, *Hum. Reprod. Update*, 2018, **24**, 119–134.

13 G. N. Subramanian, J. Greaney, Z. Wei, O. Becherel, M. Lavin and H. A. Homer, *J. Cell Biol.*, 2020, **219**, e201907213, DOI: **10.1083/jcb.201907213**.

14 J. M. Stringer, A. Winship, N. Zerafa, M. Wakefield and K. Hutta, *Proc. Natl. Acad. Sci. U. S. A.*, 2020, **117**, 11513–11522.

15 J. V. Blerkom, *Mitochondrion*, 2011, **11**, 797–813.

16 M. Benkhalifa, Y. J. Ferreira, H. Chahine, N. Louanjli, P. Miron, P. Merviel and H. Copin, *Int. J. Biochem. Cell Biol.*, 2014, **55**, 60–64.

17 P. M. Motta, S. A. Nottola, S. Makabe and R. Heyn, *Hum. Reprod.*, 2000, **15**, 129–147.

18 Z. Trebichalská, D. Kyjovská, S. Kloudová, P. Otevřel, A. Hampl and Z. Holubcová, *Biol. Reprod.*, 2020, **104**, 106–116.

19 M. T. Johnson, E. A. Freeman, D. K. Gardner and P. A. Hunt, *Biol. Reprod.*, 2007, **77**, 2–8.

20 H.-L. Xie, S. Zhu, J. Zhang, J. Wen, H.-J. Yuan, L.-Z. Pan, M.-J. Luo and J.-H. Tan, *J. Cell. Physiol.*, 2018, **233**, 6952–6964.

21 J. V. Blerkom, *Reproduction*, 2004, **128**, 269–280.

22 R. Dumollard, M. Duchen and J. Carroll, *Curr. Top. Dev. Biol.*, 2007, **77**, 21–49.

23 S. Chappel, Obstetrics and Gynecology International, 2013, pp. 1–10, DOI: **10.1155/2013/183024**.

24 Z. Roth, *J. Dairy Sci.*, 2018, **101**, 3642–3654.

25 A. J. Harvey, *Reproduction*, 2019, **157**, R159–R179.

26 K. Kim, S. Kenigsberg, A. Jurisicova and Y. Bentov, *OB*, 2019, **3**, 29.

27 N. P. Mena, O. García-Beltrán, F. Lourido, P. J. Urrutia, R. Mena, V. Castro-Castilloc, B. K. Cassels and M. T. Núñeza, *Biochem. Biophys. Res. Commun.*, 2015, **463**, 787–792.

28 N. Esteras, A. T. Dinkova-Kostova and A. Y. Abramov, *Biol. Chem.*, 2016, **397**, 383–400.

29 Y. Liu, J. Yan, C. Sun, G. Li, S. Li, L. Zhang, C. Di, L. Gan, Y. Wang, R. Zhou, J. Si and H. Zhang, *Redox Biol.*, 2018, **17**, 143–157.

30 R. J. Reiter, R. C. Carneiro and C. S. Oh, *Horm. Metab. Res.*, 1997, **29**, 363–372.

31 D.-X. Tan, L. C. Manchester, R. Hardeland, S. Lopez-Burillo, J. C. Mayo, R. M. Sainz and R. J. Reiter, *J. Pineal Res.*, 2003, **34**, 75–78.

32 A. Galano, *Phys. Chem. Chem. Phys.*, 2011, **13**, 7178–7188.

33 J. J. García, L. López-Pingarrón, P. Almeida-Souza, A. Tres, P. Escudero, F. A. García-Gil, D.-X. Tan, R. J. Reiter, J. M. Ramírez and M. Bernal-Pérez, *J. Pineal Res.*, 2014, **56**, 225–237.

34 G. J. Maarman, B. M. Andrew, D. M. Blackhurst and E. O. Ojuka, *J. Appl. Physiol.*, 2017, **122**, 1003–1010.

35 A. Tarocco, N. Caroccia, G. Morciano, M. R. Wieckowski, G. Ancora, G. Garani and P. Pinton, *Cell Death Dis.*, 2019, **10**, 317.

36 E. Absi, A. Ayala, A. Machado and J. Parrado, *J. Pineal Res.*, 2008, **29**, 40–47.

37 E. Sahna, H. Parlakpinar, N. Vardı, Y. Ciğremis and A. Acet, *Acta Histochem.*, 2004, **106**, 331–336.

38 H. Kato, G. Tanaka, S. Masuda, J. Ogasawara, T. Sakurai, T. Kizaki, H. Ohno and T. Izawa, *J. Pineal Res.*, 2015, **59**, 267–275.

39 S. A. Andrabi, I. Sayeed, D. Siemen, G. Wolf and T. F. W. Horn, *FASEB J.*, 2004, **18**, 867–897.

40 A. Jimenéz-Aranda, G. Fernández-Vázquez, M. M. A-Serrano, R. J. Reiter and A. Agil, *J. Pineal Res.*, 2014, **57**, 103–109.

41 Y. Suh, K.-A. Lee, W.-H. Kim, B.-G. Han, J. Vijg and S. C. Park, *Nat. Med.*, 2002, **8**, 3–4.

42 R. Liu, A. Fu, A. E. Hoffman, T. Zheng and Y. Zhu, *BMC Mol. Cell Biol.*, 2013, **14**(1), DOI: **10.1186/1471-2121-14-1**.

43 D. Wei, C. Zhang, J. Xie, X. Song, B. Yin, Q. Liu, L. Hu, H. Hao, J. Geng and P. Wang, *J. Assist. Reprod. Genet.*, 2013, **30**, 933–938.

44 F. Aghaz, A. Vaisi-Raygani, M. Khazaei and E. Arkan, *Biopreserv. Biobanking*, 2021, **19**, 184–193.

45 N. C. Motta, R. C. Egger, K. S. Monteiro, A. V. d. Oliveira and L. D. S. Murgas, *Theriogenology*, 2022, **179**, 14–21.

46 M. H. Karimfar, F. Niazvand, K. Haghani, S. Ghafourian, R. Shirazi and S. Bakhtiyari, *Int. J. Immunopathol. Pharmacol.*, 2015, **28**, 69–76, DOI: **10.1177/0394632015572080**.

47 E. Solanas, C. Sostres, A. Serrablo, A. García-Gil, J. J. García, F. J. Aranguren, P. Jiménez, R. D. Hughes and M. T. Serrano, *Cells Tissues Organs*, 2015, **200**, 316–325.

48 H. J. Kim, S. Lee, J. H. Lee, J. M. Park, S. J. Hong, O.-H. Lee, J. S. Park, Y. Choi and K.-H. Park, *ACS Appl. Mater. Interfaces*, 2021, **13**, 5975–5988.

49 A. C. Schroeder, A. K. Champlin, L. E. Mobraaten and J. J. Eppig, *J. Reprod. Fertil.*, 1990, **89**, 43–50.

50 J. H. Lee, J. K. Park, S. Y. Yoon, E. A. Park, J. H. Jun, H. J. Lim, J. Kim and H. Song, *Cells*, 2021, **10**, 1563.

51 L.-J. Mah, A. El-Osta and T. C. Karagiannis, *Leukemia*, 2010, **24**, 679–686.

52 M. Bang, D. G. Kim, E. L. Gonzales, K. J. Kwon and C. Y. Shin, *Biomol. Ther.*, 2019, **27**, 530–539.